International Journal of Solids and Structures 49 (2012) 853–864

Contents lists available at SciVerse ScienceDirect

International Journal of Solids and Structures

journal homepage: www.elsevier.com/locate/ijsolstr

Approximate fundamental solutions and wave fronts for general anisotropic materials

V.G. Yakhno [a,*], H. Çerdik Yaslan [b]

[a] Faculty of Engineering, Dokuz Eylul University, Kaynaklar, Buca, Izmir 35 160, Turkey
[b] Department of Mathematics, Pamukkale University, Kinikli, Denizli 20 007, Turkey

ARTICLE INFO

Article history:
Received 21 February 2011
Received in revised form 15 November 2011
Available online 3 January 2012

Keywords:
Equations of elastodynamics
Anisotropic solids
Fundamental solution
Elastic waves
Fronts
Simulation

ABSTRACT

The time-dependent differential equations of elastodynamics for homogeneous solids with a general structure of anisotropy are considered in the paper. A new method of computation of the fundamental solution for these equations is proposed. This method consists of the following. Applying the Fourier transformation with respect to space variables to these equations, we obtain a system of second order ordinary differential equations whose coefficients depend on Fourier parameters. Using the matrix transformations and properties of the coefficients, the Fourier image of the fundamental solution is computed. Finally, the fundamental solution is calculated by the inverse Fourier transformation to the obtained Fourier transform. The implementation and justification of the suggested method have been made by computational experiments in MATLAB. These experiments confirm the robustness of the suggested method. The visualization of the displacement components in general homogeneous anisotropic solids by modern computer tools allows us to see and evaluate the dependence between the structure of solids and the behavior of the displacement field. Our method allows users to observe the elastic wave propagation, arising from pulse point forces of the form $\mathbf{e}^m\delta(x)\delta(t)$, in monoclinic, triclinic and other anisotropic solids. The visualization of displacement components gives knowledge about the form of fronts of elastic wave propagation in Sodium Thiosulfate with monoclinic and Copper Sulphate Pentahydrate with triclinic structures of anisotropy.

1. Introduction

Many applied problems of structural mechanics, geophysics, material sciences are closely related to study of the wave propagation in anisotropic elastic materials and media, arising from impulsive loadings and forces located at one or several points (see, for example, Aki and Richards, 1980; Carcione, 2001; Ting et al., 1990; Ting, 1996; Harada and Sasahara, 2009; Hachemi et al., 2008; Dieulesaint and Royer, 1980; Freund, 1998; Fedorov, 1968). The behavior of the wave processes essentially depends on properties of materials and media (density and elastic moduli). It can be noted, that the forms of wave fronts from the pulse point sources in elastic materials with general structure of anisotropy (monoclinic, triclinic) are not spherical and have very peculiar forms. The computation of the displacement is complicated because the displacements are generalized functions (distributions) (see Vladimirov, 1971, 1979; Reed and Simon, 1975; Hormander, 1963).

The differential equations of anisotropic elastodynamics describe the dynamic processes of the wave phenomena in anisotropic materials and media. The problems of elastodynamics are often stated in the form of computing displacement components at internal points of anisotropic solids. Analytical and numerical methods play the important role in the study of these problems (see, for example, Poruchikov, 1993; Chang and Wu, 2003; Carrer and Mansur, 1999; Sladek et al., 2005; Moosavi and Khelil, 2009; Dauksher and Emery, 2000). Besides that, fundamental solutions (Green's functions) of equations of elastodynamics are important tools for solving these problems (see for example, Mansur and Loureiro, 2009; Mansur et al., 2007; Soares and Mansur, 2005; Vera-Tudela and Telles, 2005; Rangelov et al., 2005; Rangelov, 2003; Berger and Tewary, 1996; Tewary, 1995; Wang and Achenbach, 1994, 1995).

The existence proofs for fundamental solutions in the spaces of generalized functions for any linear differential equations with constant coefficients were given by Malgrange (1955–1956), Ehrenpreis (1960) and Hormander (1963). Ignoring here many approaches of finding fundamental solutions for scalar differential equations with constant coefficients, we point out only some of methods for equations of elastodynamics. The analytical

* Corresponding author.
E-mail addresses: valery.yakhno@deu.edu.tr (V.G. Yakhno), hcerdik@pau.edu.tr (H. Çerdik Yaslan).

0020-7683/$ - see front matter © 2011 Elsevier Ltd. All rights reserved.
doi:10.1016/j.ijsolstr.2011.12.010

computation of the explicit formulae for fundamental solutions in homogeneous isotropic linearly elastic solids offers no difficulty (see, for example, Aki and Richards, 1980; Payton, 1983). But this is not the case for general homogeneous anisotropic media. The methods of fundamental solutions construction for dynamic equations of linear anisotropic elasticity have been developed by Wang and Achenbach (1994, 1995), Tewary (1995), Wang et al. (2007), Khojasteh et al. (2008), Rangelov et al. (2005), Rangelov (2003), Vavrycuk (2001), Vavrycuk (2002), Garg et al. (2004) and other authors. The fundamental solutions of anisotropic elasticity mentioned above are either approximations or have complicated mathematical forms, which are difficult to evaluate numerically for general anisotropic media (monoclinic, triclinic). Most of approaches are related with the Fourier–Laplace presentation in a wave-vector-frequency space. In this case the inverse Fourier–Laplace representation for the fundamental solutions requires 4D integration over functions with singularities. The oscillatory nature of the Fourier–Laplace representation of fundamental solutions and calculation of the principal value at the singularities create computational difficulties.

An interesting approach for finding fundamental solutions by the Radon transform for 3D and 2D time-domain elastodynamics has been suggested by Wang and Achenbach (1994). They found fundamental solutions in the form of a surface integral over a unit sphere for a 3D case. Physically, the integral can be interpreted as a superposition of plane waves, propagating in all directions. The resulting expression has a complicated form containing integration over the slowness surface. The presentation of a fundamental solution as an integral over slowness surfaces dates back to Burridge et al. (1993). We note that for some anisotropic materials (cubic, transversely isotropic) fundamental solutions can be evaluated numerically using this approach (see Wang and Achenbach, 1994), but not for the case of general homogeneous anisotropic solids with monoclinic and triclinic structures of anisotropy, because slowness surfaces are complicated.

In the paper Tewary (1995), the formula for the time-dependent fundamental solution in three dimensional anisotropic elastic infinite solids has been derived by the Radon transform and solving the Christoffel equation in terms of the delta function. Computational advantages of this method are the following: it does not require integration over frequency; the integration is made over two of three variables. But the numerical realization of this method for general (triclinic, monoclinic, etc.) anisotropic elastic solids is questionable, because it is not clear how to compute the weight function in the obtained Radon representation.

The numerical computation of fundamental solutions for general linear equations of elastodynamics with three space and one time variables has been obtained only for particular cases of anisotropy such as cubic, isotropic, transversely isotropic, orthotropic structures (Wang and Achenbach, 1994, 1995; Tewary, 1995; Yang et al., 2004; Rangelov, 2003; Kocak and Yildirim, 2009; Khojasteh et al., 2008). The complete numerical computation of fundamental solutions in such anisotropic elastic media as trigonal, monoclinic, triclinic has not been done so far. The problem of the fundamental solution calculation for equations of elastodynamics with the general structure of anisotropy is rather complicated. The complexity depends on the characteristics of material media (density and elastic moduli) and boundary conditions. In the case of a free-space the boundaries are not present. However, even with this simplification, the numerical computation of fundamental solutions for general anisotropic media was not known till the last decade.

In the latest paper of Yakhno and Cerdik Yaslan (2011) the equations of elastodynamics have been written in the form of the symmetric hyperbolic system of the first order relative to the components of the speed of the displacement and stresses. The problem of finding the approximate speed of displacement and stresses, arising from the directional pulse point force in anisotropic media, has been formulated. The authors have suggested a method of calculation of the components of the speed of the displacement and stresses by solving this hyperbolic system.The fundamental solution of this hyperbolic system has been computed. Using this fundamental solution, the components of the fundamental solution of the original second order equations of elastodynamics have been calculated by additional integration with respect to the time variable. The empirical comparison of the results with explicit formulae of isotropic materials has demonstrated meaningfulness of the approach.

Unfortunately, this system has contained nine coupled equations, that made the procedure of calculation of the fundamental solution cumbersome, and together with additional integration, led to the loss of accuracy in numerical calculations. To overcome these difficulties the authors have worked out a new method for the direct calculation of the displacement from original second order equations of elastodynamics, which is described in the present paper.

This method consists in the following: the second order equations of elastodynamics have been written in terms of the Fourier transform with respect to the space variables as a system of the ordinary differential equations of the second order with coefficients depending on the Fourier parameters. The solution of the obtained system has been derived by the matrix transformations and technique of the ordinary differential equations. After that the inverse Fourier transformation has been applied numerically to this solution.

This method has the advantage of simplicity of its numerical realization for general homogeneous anisotropic solids with monoclinic and triclinic structures of anisotropy as well as numerical computation of the displacement fields, arising from pulse point forces in these anisotropic solids. Moreover, using our method, a visualization of the behavior of elastic fields, arising from pulse point forces in monoclinic and triclinic anisotropic solids has been made. As a result, new knowledge about forms of fronts of elastic waves in Sodium Thiosulfate with monoclinic and Copper Sulphate Pentahydrate with triclinic structures of anisotropy has been obtained.

The paper is organized as follows. In Section 2 the equations of elastodynamics for linear anisotropic solids are written in the form of a vector second order partial differential equation and the time-dependent FS of equations of elastodynamics is defined by means of this vector equation. The derivation of a formula for an arbitrary column of the FS is given in Section 3. Justification of our method and computational experiments are described in Section 4.

2. The fundamental solution of equations of linear anisotropic elastodynamics

Let $x = (x_1, x_2, x_3) \in R^3$ be a space variable, $t \in R$ be a time variable. Let us consider an unbounded, homogeneous anisotropic linearly elastic solid in the Cartesian coordinate system $x = (x_1, x_2, x_3)$. The solid is defined by the mass density $\rho > 0$ and the elastic constants C_{ijkl}, $i, j, k, l = 1, 2, 3$, which are fully symmetric and positive definite, i.e.

$$C_{ijkl} = C_{jikl} = C_{ijlk} = C_{klij} \tag{1}$$

and

$$\sum_{i,j,k,l=1}^{3} C_{ijkl}\varepsilon_{ij}\varepsilon_{kl} > 0 \tag{2}$$

for any non-zero real symmetric tensor ε_{ij}. Let $\mathbf{u}(x,t) = (u_1(x,t), u_2(x,t), u_3(x,t))$ be the displacement vector; $\sigma_{ij}(x,t)$ be the stresses defined by

$$\sigma_{ij}(x,t)=\sum_{k,l=1}^{3}c_{ijkl}\frac{\partial u_k}{\partial x_l},\quad i,j=1,2,3. \tag{3}$$

The dynamical model of the elastic wave propagation in the considered anisotropic media, arising from the force $\mathbf{g}(x,t)=(g_1(x,t), g_2(x,t), g_3(x,t))$, is given by the following motion equations (see, for example, Aki and Richards, 1980; Dieulesaint and Royer, 1980; Fedorov, 1968)

$$\rho\frac{\partial^2 u_i(x,t)}{\partial t^2}=\sum_{j=1}^{3}\frac{\partial\sigma_{ij}(x,t)}{\partial x_j}+g_i(x,t). \tag{4}$$

The motion Eq. (4) can be written in the following vector form

$$\rho\frac{\partial^2\mathbf{u}(x,t)}{\partial t^2}=\sum_{j,l=1}^{3}\mathbf{A}_{jl}\frac{\partial^2\mathbf{u}(x,t)}{\partial x_j\partial x_l}+\mathbf{g}(x,t), \tag{5}$$

where $\mathbf{A}_{jl}j$, $l=1,2,3$ are matrices defined by

$$\mathbf{A}_{jl}=\begin{bmatrix}C_{1j1l} & C_{1j2l} & C_{1j3l}\\ C_{2j1l} & C_{2j2l} & C_{2j3l}\\ C_{3j1l} & C_{3j2l} & C_{3j3l}\end{bmatrix}. \tag{6}$$

Let us consider the point forces of the form $\mathbf{e}^m\delta(x)\,f(t)$, where $m=1,2,3$; $\mathbf{e}^1=(1,0,0)$, $\mathbf{e}^2=(0,1,0)$, $\mathbf{e}^3=(0,0,1)$ are basis vectors of the space R^3; $\delta(x)=\delta(x_1)\cdot\delta(x_2)\cdot\delta(x_3)$ is the $3D$ Dirac delta function concentrated at the point $(0,0,0)$ from R^3; $f(t)$ is a function such that $f(t)=0$ for $t<0$.

Let $\mathbf{u}^m(x,t)=(u_1^m(x,t),u_2^m(x,t),u_3^m(x,t))$ be a solution of (5) for $\mathbf{g}(x,\ t)=\mathbf{e}^m\delta(x)f(t)$, satisfying $\mathbf{u}^m(x,t)|_{t<0}=0$, i.e.

$$\rho\frac{\partial^2\mathbf{u}^m(x,t)}{\partial t^2}=\sum_{j,l=1}^{3}\mathbf{A}_{jl}\frac{\partial^2\mathbf{u}^m(x,t)}{\partial x_j\partial x_l}+\mathbf{e}^m\delta(x)f(t), \tag{7}$$

$$\mathbf{u}^m(x,t)|_{t<0}=0. \tag{8}$$

It can be noted that the problem of determination of a generalized function, satisfying the time-dependent partial differential equations, for example (7) subject to a causality condition (8), is very often called the generalized Cauchy problem (see, for example, Vladimirov, 1971, pp. 172–178). If $f(t)=\delta(t)$ then the causality condition (8) is one of necessary conditions to define the time-dependent fundamental solution (Green's function) for the hyperbolic equation (7) (see, for example, Barton, 1991, pp. 262–290)

The time-dependent fundamental solution of equations of linear anisotropic elastodynamics is defined as a matrix $\mathcal{G}(x,t)$ of the order 3×3 whose columns $\mathbf{G}^m(x,t)=(G_1^m(x,t),G_2^m(x,t),G_3^m(x,t))$, $m=1,2,3$ satisfy (7) and (8) for $f(t)=\delta(t)$, where $\delta(t)$ is the $1D$ Dirac delta function concentrated at $t=0$. From physical point of view, the mth column of the fundamental solution of equations of linear anisotropic elastodynamics is the displacement, arising from the pulse point force $\mathbf{e}^m\delta(x)\delta(t)$. The method for computation of the vector function $\mathbf{u}^m(x,t)$, satisfying (7) and (8) is the main focus of this paper.

3. Computation of the solution of the generalized Cauchy problem (7) and (8)

The method consists of the following. In the first step Eqs. (7) and (8) are written in terms of the Fourier transform with respect to $x\in R^3$. In the second step, a solution of the obtained initial value problem is derived by matrix transformations and the ordinary differential equations technique. In the last step, the solution of (7) and (8) is found by the inverse Fourier transformation.

3.1. Eqs. (7) and (8) in terms of Fourier transform

Let $\tilde{\mathbf{u}}^m(v,t)=(\tilde{u_1}^m(v,t),\tilde{u_2}^m(v,t),\tilde{u_3}^m(v,t))$ be the Fourier image of $\mathbf{u}^m(x,t)$ with respect to $x=(x_1,x_2,x_3)\in R^3$, i.e.

$$\tilde{u_j}^m(v,t)=F_x[u_j^m(x,t)](v),$$

$$F_x[u_j^m(x,t)](v)=\int_{-\infty}^{\infty}\int_{-\infty}^{\infty}\int_{-\infty}^{\infty}u_j^m(x,t)e^{ix\cdot v}\,dx_1\,dx_2\,dx_3,$$

where $i^2=-1$, $j=1,2,3$,

$$v=(v_1,v_2,v_3)\in R^3,\quad x\cdot v=x_1v_1+x_2v_2+x_3v_3.$$

Eqs. (7) and (8) can be written in terms of $\tilde{\mathbf{u}}^m(v,t)$ as follows

$$\rho\frac{d^2\tilde{\mathbf{u}}^m}{dt^2}+\mathbf{A}(v)\tilde{\mathbf{u}}^m=\mathbf{e}^m f(t),\quad v\in R^3,\quad t\in R, \tag{9}$$

$$\tilde{\mathbf{u}}^m(v,t)|_{t<0}=0. \tag{10}$$

Here

$$\mathbf{A}(v)=\sum_{j,l=1}^{3}\mathbf{A}_{jl}v_jv_l, \tag{11}$$

where matrices $\mathbf{A}_{jl}$ are defined by (6).

3.2. Derivation of the solution of (9) and (10)

The solution of (9) and (10) for $v_1=0$, $v_2=0$, $v_3=0$ is given by

$$\tilde{\mathbf{u}}^m(0,t)=\frac{\theta(t)}{\rho}\left(\int_0^t(t-\tau)f(\tau)\,d\tau\right)\mathbf{e}^m, \tag{12}$$

where $\theta(t)$ is the Heaviside function, i.e. $\theta(t)=1$ for $t\geqslant0$ and $\theta(t)=0$ for $t<0$.

For $v\neq0$, using the symmetry and positivity of elastic constants C_{ijkl}(see conditions (1)), we obtain that the matrix $\mathbf{A}(v)$, defined by (11), is symmetric positive definite. For the given matrix $\mathbf{A}(v)$ we construct an orthogonal matrix $\mathcal{T}(v)$ and a diagonal matrix $\mathbf{D}(v)=diag(d_k(v),\ k=1,2,3)$ with positive elements, such that

$$\mathcal{T}^*(v)\mathbf{A}(v)\mathcal{T}(v)=\mathbf{D}(v), \tag{13}$$

where $\mathcal{T}^*(v)$ is the transposed matrix to $\mathcal{T}(v)$.

Let $\mathcal{T}(v)$ and $\mathbf{D}(v)=diag(d_k(v),\ k=1,2,3)$ be constructed. The solution of (9) and (10) can be found as

$$\tilde{\mathbf{u}}^m(v,t)=\mathcal{T}(v)\mathbf{Y}^m(v,t), \tag{14}$$

where $\mathbf{Y}^m(v,t)$ is unknown vector function. Substituting (14) into (9) and (10) and then multiplying the obtained equations by $\mathcal{T}^*(v)$ and from (13), we find

$$\rho\frac{d^2\mathbf{Y}^m}{dt^2}+D(v)\mathbf{Y}^m=\mathcal{T}^*(v)\mathbf{e}^m f(t), \tag{15}$$

$$\mathbf{Y}^m(v,t)|_{t<0}=0,\quad t\in R,\quad v\in R^3. \tag{16}$$

Using the standard technique (see, for example, Vladimirov, 1971, p. 147), we derive the solution of the generalized Cauchy problem (15) and (16) for $d_k(v)>0$ in explicit form:

$$\mathbf{Y}_k^m(v,t)=\theta(t)\int_0^t\frac{[\mathcal{T}^*(v)\mathbf{e}^m]_k f(\tau)}{\sqrt{\rho d_k(v)}}\sin\left((t-\tau)\sqrt{\frac{d_k(v)}{\rho}}\right)d\tau. \tag{17}$$

Finally, a solution of (9) and (10) is determined by (12), (14) and (17).

3.3. The formula of the Fourier transform of the fundamental solution

The Fourier transform of the fundamental solution of equations of linear anisotropic elastodynamics is a matrix of the order 3×3,

whose columns $\widetilde{\mathbf{G}}^m(y,t)=\left(\widetilde{G}_1^m(y,t),\widetilde{G}_2^m(y,t),\widetilde{G}_3^m(y,t)\right)$, $m=1,2,3$ satisfy

$$\rho\frac{d^2\widetilde{\mathbf{G}}^m}{dt^2}+\mathbf{A}(y)\widetilde{\mathbf{G}}^m=\mathbf{e}^m\delta(t), \tag{18}$$

$$\widetilde{\mathbf{G}}^m(y,t)|_{t<0}=0,\quad y\in R^3,\quad t\in R. \tag{19}$$

Similar to the Section 3.1 we find $\widetilde{\mathbf{G}}^m(0,t)$ by

$$\widetilde{\mathbf{G}}^m(0,t)=\frac{\theta(t)}{\rho}t\mathbf{e}^m, \tag{20}$$

and we compute $\widetilde{\mathbf{G}}^m(y,t)$ for $y\neq 0$ as follows

$$\widetilde{\mathbf{G}}^m(y,t)=\mathcal{T}(y)\mathbf{Y}^m(y,t), \tag{21}$$

where components of

$$\mathbf{Y}^m(y,t)=\left(Y_1^m(y,t),Y_2^m(y,t),Y_3^m(y,t)\right)$$

are given by

$$\mathbf{Y}_k^m(y,t)=\theta(t)\frac{[\mathcal{T}^*(y)\mathbf{e}^m]_k}{\sqrt{\rho d_k(y)}}\sin\left(\sqrt{\frac{d_k(y)}{\rho}}t\right). \tag{22}$$

3.4. Formulae for the solution of (9) and (10)

When the Fourier transform of the fundamental solution is calculated, it becomes possible to apply the inverse Fourier transformation in a sense of tempered distributions. Such approach can be found in the books Vladimirov (1971) and Hormander (1963).

Let $\tilde{\mathbf{u}}^m(y,t)$ be the solution of (9) and (10) defined by (12), (14) and (17). The solution $\mathbf{u}^m(x,t)$ of (7) and (8) is defined by the inverse Fourier transform of $\tilde{\mathbf{u}}^m(y,t)$, i.e. by the formula

$$\begin{aligned}&\mathbf{u}^m(x,t)=F_y^{-1}[\tilde{\mathbf{u}}^m(y,t)](x),\\ &F_y^{-1}[\tilde{\mathbf{u}}^m(y,t)](x)=\frac{1}{(2\pi)^3}\int_{-\infty}^{+\infty}\int_{-\infty}^{+\infty}\int_{-\infty}^{+\infty}\tilde{\mathbf{u}}^m(y,t)e^{-ix\cdot y}\,dy_1\,dy_2dy_3,\\ &y=(y_1,y_2,y_3)\in R^3,\quad x=(x_1,x_2,x_3)\in R^3.\end{aligned} \tag{23}$$

Taking into account that the components of the vector function $\mathbf{u}^m(x,t)$ as well as the components of vector functions $\tilde{\mathbf{u}}^m(y,t)$ have real values, the imaginary part of the right hand side of (23) is equal to zero. As a result, we find the following formula for the solution of (9) and (10) from (23):

$$\begin{aligned}\mathbf{u}^m(x,t)=\frac{\theta(t)}{(2\pi)^3}&\int_{-\infty}^{\infty}\int_{-\infty}^{\infty}\int_{-\infty}^{\infty}\tilde{\mathbf{u}}^m(y,t)\cos(x_1y_1+x_2y_2\\ &+x_3y_3)\,dy_1\,dy_2\,dy_3.\end{aligned} \tag{24}$$

Using the similar reasonings and formulae (20) and (21) we obtain the formula for mth column of the fundamental solution

$$\begin{aligned}\mathbf{G}^m(x,t)=\frac{\theta(t)}{(2\pi)^3}&\int_{-\infty}^{\infty}\int_{-\infty}^{\infty}\int_{-\infty}^{\infty}\widetilde{\mathbf{G}}^m(y,t)\cos(x_1y_1+x_2y_2\\ &+x_3y_3)\,dy_1\,dy_2\,dy_3,\end{aligned} \tag{25}$$

where $\widetilde{\mathbf{G}}^m(y,t)$ is defined by (20)–(22).

It can be noted, that the integrals (24) and (25) can not be calculated by symbolic transformations for the general anisotropic media.

3.5. Numerical computation of 3D inverse Fourier transformation

The computation of the 3D integrals (24) and (25) has been done numerically over a bounded domain $(-A,A)\times(-A,A)\times(-A,A)$, where $A>0$ is a parameter. As a result, we have got a regularized (approximate) solution of the fundamental solution with the parameter of regularization A. This solution approaches the fundamental solution as the parameter A tends to ∞ in the sense of tempered distributions (see Vladimirov, 1971; Hormander, 1963).

To select the parameter A, we have used the explicit formula of the fundamental solution of isotropic elastodynamics.

The explicit formula of the fundamental solution of equations of isotropic elastodynamics is well known (see, for example, Aki and Richards, 1980). For example, components of the first column of the fundamental solution can be written in the form

$$\begin{aligned}G_1^1(x_1,x_2,x_3,t)=&\frac{1}{4\pi\rho}\left(\frac{3x_1^2}{|x|^5}-\frac{1}{|x|^3}\right)\theta\left(t-\frac{|x|}{C_L}\right)\theta\left(\frac{|x|}{C_T}-t\right)t\\ &+\frac{1}{4\pi\rho C_P^2}\frac{x_1^2}{|x|^3}\delta\left(t-\frac{|x|}{C_L}\right)\\ &+\frac{1}{4\pi\rho C_T^2|x|}\left(1-\frac{x_1^2}{|x|^2}\right)\delta\left(t-\frac{|x|}{C_T}\right),\end{aligned} \tag{26}$$

$$\begin{aligned}G_2^1(x_1,x_2,x_3,t)=&\frac{1}{4\pi\rho}\frac{3x_1x_2}{|x|^5}\theta\left(t-\frac{|x|}{C_L}\right)\theta\left(\frac{|x|}{C_T}-t\right)t+\frac{1}{4\pi\rho C_L^2}\\ &\times\frac{x_1x_2}{|x|^3}\delta\left(t-\frac{|x|}{C_L}\right)\\ &-\frac{1}{4\pi\rho C_T^2}\left(\frac{x_1x_2}{|x|^3}\right)\delta\left(t-\frac{|x|}{C_T}\right),\end{aligned} \tag{27}$$

$$\begin{aligned}G_3^1(x_1,x_2,x_3,t)=&\frac{1}{4\pi\rho}\frac{3x_1x_3}{|x|^5}\theta\left(t-\frac{|x|}{C_L}\right)\theta\left(\frac{|x|}{C_T}-t\right)t+\frac{1}{4\pi\rho C_L^2}\\ &\times\frac{x_1x_3}{|x|^3}\delta\left(t-\frac{|x|}{C_L}\right)\\ &-\frac{1}{4\pi\rho C_T^2}\left(\frac{x_1x_3}{|x|^3}\right)\delta\left(t-\frac{|x|}{C_T}\right).\end{aligned} \tag{28}$$

These formulae contain singular terms $\delta(C_Tt-|x|)/(4\pi C_T^2\rho|x|)$ and $\delta(C_Lt-|x|)/(4\pi C_L^2\rho|x|)$. The supports of these singular terms are the characteristic cones $tC_T=|x|$ and $tC_L=|x|$ in the space of variables x_1, x_2, x_3, t. Usually the classical functions are defined by the point-wise manner and we can draw their graphs. Unfortunately, this point-wise definition and its graphic presentation is not adequate to singular generalized functions (Vladimirov, 1979; Vladimirov, 1971; Reed and Simon, 1975). For this reason they are very often replaced by regularized functions which are classical and have graphic presentations. This regularization has a parameter of the regularization and the singular generalized function is a limit in the sense of the generalized functions space, when the parameter of this regularization tends to $+\infty$ (or $+0$). For example, the singular generalized function $\delta(t)$ can be regularized by $\frac{1}{2\sqrt{\pi\varepsilon}}\exp\left(-t^2/(4\varepsilon)\right)$and the singular generalized function $\delta(C_Tt-|x|)$ by $\frac{1}{2\sqrt{\pi\varepsilon}}\exp\left[-(C_Tt-|x|)^2/(4\varepsilon)\right]$ (see Vladimirov, 1979).

On the other hand $\delta(C_Tt-|x|)/(4\pi C_T^2\rho|x|)$ can be regularized by

$$\begin{aligned}&h_A(x,t)=\frac{1}{(2\pi)^3}\int_{-A}^{A}\int_{-A}^{A}\int_{-A}^{A}\frac{\sin(C_T|y|t)}{\rho C_T|y|}e^{-ix\cdot y}\,dy_1\,dy_2\,dy_3,\quad t>0,\\ &i^2=-1,\quad y=(y_1,y_2,y_3)\in R^3,\quad x=(x_1,x_2,x_3)\in R^3,\\ &x\cdot y=x_1y_1+x_2y_2+x_3y_3.\end{aligned} \tag{29}$$

We know that (see Vladimirov, 1979)

$$\begin{aligned}&\lim_{A\to+\infty}\frac{1}{(2\pi)^3}\int_{-A}^{A}\int_{-A}^{A}\int_{-A}^{A}\frac{\sin(C_T|y|t)}{\rho C_T|y|}e^{-ixy}dy_1dy_2dy_3\\ &=F_y^{-1}\left[\frac{\sin(C_T|y|t)}{\rho C_T|y|}\right](x)\end{aligned}$$

and

$$F_v^{-1}\left[\frac{\sin(C_T|v|t)}{\rho C_T|v|}\right](x)=\frac{1}{4\pi C_T^2|x|\rho}\delta(C_Tt-|x|).$$

Here F_v^{-1} is the 3D inverse Fourier transform defined by (23). Since the function $\sin(C_T|v|t)/(\rho C_T|v|)$ is even, we can replace the 3D integral of (29) by

$$\int_{-A}^{A}\int_{-A}^{A}\int_{-A}^{A}\frac{\sin(C_T|v|t)}{\rho C_T|v|}\cos(x\cdot v)\,dv_1\,dv_2\,dv_3$$

and then approximate the obtained integral by the following triple sums

$$\sum_{n=-N}^{N}\sum_{m=-N}^{N}\sum_{l=-N}^{N}\frac{\sin(C_T|v|t)}{\rho C_T|v|}\Big|_{v=(n\Delta v,m\Delta v,l\Delta v)}\cos(\Delta v(nx_1+mx_2+lx_3))(\Delta v)^3,$$

where N is a natural number for which $A=N\Delta v$ and real numbers A and Δv have been chosen from empirical observations and natural logic. Namely, using the obtained integral sums we compute the values of $h_A(x,t)$ for $\Delta v=1$, $\Delta v=0.5$, $\Delta v=0.025$, $A=20$, $A=30$, $A=40$, $A=50$ and so forth numerically in MATLAB. The results of computation have been compared with the values of the function $\frac{1}{2\sqrt{\pi\varepsilon}}\exp\left[-(C_Tt-|x|)^2/(4\varepsilon)\right]/(4\pi C_T^2\rho|x|)$ $(\varepsilon=0.0001)$, which is a regularization of $\delta(C_Tt-|x|)/(4\pi C_T^2\rho|x|)$. We have observed that the difference between values of $h_A(x,t)$ and $\frac{1}{2\sqrt{\pi\varepsilon}}\exp[-(C_Tt-|x|)^2/(4\varepsilon)]/(4\pi C_T^2\rho|x|),(\varepsilon=0.0001)$, corresponding to $\Delta v=0.5$ and $A=40$, $A=50$, $A=60$, $A=70$, becomes small and the increment of the regularization for the parameter A is not essential according to the case $\Delta v=0.5$, $A=40$. For this reason, we have chosen $\Delta v=0.5$, $A=40$ as suitable parameters for $h_A(x,t)$ for regularization of $\delta(C_Tt-|x|)/(4\pi C_T^2\rho|x|)$ by the 3D integral sum.

4. Computational experiments: implementation and justification

For validation of the method the different types of computational experiments have been implemented. First, we have compared the results of calculation of the Fourier transform with the values obtained from the explicit formulae for the isotropic material and anisotropic one with cubic structure. The second type of experiments compares the calculated values of the displacement vectors with values, obtained by the method of Wang and Achenbach (1994), as well as with values obtained from the explicit formulae for the isotropic material Silica (SiO_2), derived by Aki and Richards (1980).

The last group of experiments calculates and draws the images of the wave propagation in materials with the general structure of anisotropy.

4.1. Comparison of the Fourier transforms

The fundamental solution is a singular generalized function (distribution) with a compact support for a fixed time variable. Physically it means that the perturbation from the pulse point force propagates in a bounded domain of isotropic or anisotropic indefinite solids for a fixed time and therefore there is a quiet in all points outside this bounded domain.

The accuracy of the approximation of the fundamental solutions of the time-dependent equations of elastodynamics can not be quantified in principle, because the concepts of norm and metric are not defined in the space of generalized functions (see Vladimirov, 1979). Using the Paley–Wiener theorem (see, for example, Reed and Simon, 1975) we obtain that the Fourier transform of the fundamental solution with respect to space variables is an analytic function of the Fourier parameters for the bounded time interval. That is why it becomes possible to evaluate the accuracy of the approximation of the Fourier transform of the fundamental solution.

For the comparison we have considered two materials with explicit formulae for the Fourier transform of their fundamental solutions. The first one is the isotropic material, the second one – anisotropic with the cubic structure.

4.1.1. Isotropic material

We have considered the isotropic material silica (SiO_2) characterized by the density $\rho=2.203$ $(10^3\ \mathrm{kg/m^3})$ and Lame parameters $\lambda=1.61$, $\mu=3.12$ $(10^{10}\ \mathrm{Pa})$ (see, for example, Dieulesaint and Royer, 2000, p. 163). For this computational experiment we take the pulse point force $\mathbf{e}^3\delta(x_1)\delta(x_2)\delta(x_3)\delta(t)$, where $\mathbf{e}^3=(0,0,1)$. Applying our method, we have computed $\mathcal{T}(v),\mathcal{T}^*(v)$, $D(v)$ and then using the formula (20)–(22) we find the third column of the Fourier transform of the fundamental solution $\widetilde{\mathbf{G}}^m(v,t)$ for arbitrary $v=(v_1,v_2,v_3)\in R^3$ and any fixed time t. On the other hand, for this material there exists the explicit formulae (see, for example, Aki and Richards, 1980). If we denote the fundamental solution of equations of isotropic elastodynamics by 3×3 matrix $\mathcal{E}(x,t)$ with columns $\mathbf{E}^m(x,t)=(E_1^m(x,t),E_2^m(x,t),E_3^m(x,t))$ and the Fourier transform of $\mathcal{E}(x,t)$ by 3×3 matrix $\widetilde{\mathcal{E}}(v,t)$ with columns $\widetilde{\mathbf{E}}^m(v,t)=\left(\widetilde{E}_1^m(v,t),\widetilde{E}_2^m(v,t),\widetilde{E}_3^m(v,t)\right)$ then, for example, for components of the third column $\widetilde{\mathbf{E}}^3(v,t)$ the following explicit formulae hold

$$\widetilde{E}_1^3(v,t)=\frac{\theta(t)}{\rho|v|^3}v_1v_3\left(\frac{\sin(C_L|v|t)}{C_L}-\frac{\sin(C_T|v|t)}{C_T}\right),\tag{30}$$

$$\widetilde{E}_2^3(v,t)=\frac{\theta(t)}{\rho|v|^3}v_2v_3\left(\frac{\sin(C_L|v|t)}{C_L}-\frac{\sin(C_T|v|t)}{C_T}\right),\tag{31}$$

$$\widetilde{E}_3^3(v,t)=\frac{\theta(t)}{\rho|v|^3}\left(\frac{\sin(C_L|v|t)}{C_L}v_3^2+\frac{\sin(C_T|v|t)}{C_T}(v_1^2+v_2^2)\right),\tag{32}$$

where $C_T^2=\mu/\rho$, $C_L^2=(\lambda+2\mu)/\rho$.

Using our method and the explicit formulae (30)–(32) we have computed values $\widetilde{\mathbf{G}}^3(v,t)$ and $\widetilde{\mathbf{E}}^3(v,t)$. Some values of $\widetilde{G}_3^3(v,t)$ and $\widetilde{G}_3^3(v,t)-\widetilde{E}_3^3(v,t)$ are given in Table 1. Moreover, we have considered $\widetilde{G}_3^3(v,t)$ and $\widetilde{E}_3^3(v,t)$ for $v_1=v_2=v_3=y$ and $t=1$ as two functions of one variable $y\in R$. The graphs of these functions are presented in Fig. 1, where the horizontal axis is the axis of the variable y and the vertical axis is values of the considered functions.

The results of this computational experiment have shown that values of the Fourier transform found by our method and by the explicit formulae are almost the same (the accuracy in this experiment is less or equal to 10^{-16}).

4.1.2. Anisotropic material of the cubic structure

In this section we consider the material Gold, which has the cubic crystalline structure. This material is characterized by the density $\rho=19.3$ $(10^3\ \mathrm{kg/m^3})$, and elastic modules $c_{1111}=c_{2222}=c_{3333}=19.25$ $(10^{10}\ \mathrm{Pa})$, $c_{1122}=c_{1133}=c_{2233}=c_{2211}=c_{3311}=c_{3322}=16.3$ $(10^{10}\ \mathrm{Pa})$, $c_{2323}=c_{1313}=c_{1212}=c_{2323}=c_{3232}=c_{2332}=c_{3223}=c_{3131}=c_{3113}=c_{1331}=c_{2121}=c_{2112}=c_{1221}=4.24$ $(10^{10}\ \mathrm{Pa})$. Other modules are equal to zero.

Let λ be the number defined as $\lambda=\frac{c_{1111}-c_{2323}}{c_{1122}+c_{2323}}$. Let $\mathbf{u}^m(x,t)$ be the mth column of the fundamental solution for this medium. We note that $\mathbf{u}^m(x,t)$ has to satisfy (7) and (8). Applying the Fourier transform with respect to $x=(x_1,x_2,x_3)\in R^3$ to (7) and (8) we have obtained for this anisotropic medium the following equation

$$\rho\frac{\partial^2\widetilde{\mathbf{u}}^m}{\partial t^2}+(c_{1122}+c_{2323})P(v)\widetilde{\mathbf{u}}^m+c_{2323}|v|^2\widetilde{\mathbf{u}}^m=\mathbf{e}^m\delta(t),\tag{33}$$

$$\widetilde{\mathbf{u}}^m(v,t)|_{t<0}=0,\tag{34}$$

Table 1
The accuracy of computing $\widetilde{G}_3^3(v,t)$ in isotropic material silica (SiO_2).

t	v_1	v_2	v_3	$\widetilde{G}_3^3(v,t)$	$\widetilde{G}_3^3(v,t)-\widetilde{E}_3^3(v,t)$
1	10^{-5}	10^{-5}	10^{-5}	0.4539264639	-0.1×10^{-15}
	10^{-5}	10^{-4}	10^{-3}	0.4539261932	-0.1×10^{-15}
	10^{-4}	10^{-4}	10^{-4}	0.4539264591	0.6×10^{-16}
	10^{-3}	10^{-3}	10^{-3}	0.4539259800	0.1×10^{-15}
	10^{-2}	10^{-2}	10^{-2}	0.4538780786	0
	10^{-1}	10^{-2}	10^{-3}	0.4528447980	0
	10^{-1}	10^{-1}	10^{-1}	0.4491066612	0
	1	1	1	0.1236007290	0.6×10^{-16}
	10^{1}	10^{1}	10^{1}	$0.1884405489\times10^{-1}$	-0.3×10^{-17}
	10^{2}	10^{2}	10^{2}	$-0.1273480138\times10^{-2}$	-0.4×10^{-16}
	10^{1}	10^{2}	10^{3}	$-0.7528755459\times10^{-4}$	-0.5×10^{-16}
	10^{3}	10^{3}	10^{3}	$0.8709300174\times10^{-4}$	-0.4×10^{-16}
	10^{5}	10^{4}	10^{3}	$-0.3012966019\times10^{-5}$	-0.3×10^{-16}
2	10^{-5}	10^{-5}	10^{-5}	0.9078529274	-0.1×10^{-15}
	10^{-5}	10^{-4}	10^{-3}	0.9078507625	-0.2×10^{-15}
	10^{-4}	10^{-4}	10^{-4}	0.9078528891	0
	10^{-3}	10^{-3}	10^{-3}	0.9078490569	0.1×10^{-15}
	10^{-2}	10^{-2}	10^{-2}	0.9074658907	-0.1×10^{-15}
	10^{-1}	10^{-2}	10^{-3}	0.8992181580	-0.2×10^{-15}
	10^{-1}	10^{-1}	10^{-1}	0.8697446556	0
	1	1	1	−0.1102871416	0.1×10^{-16}
	10^{1}	10^{1}	10^{1}	$-0.2958623228\times10^{-2}$	0.5×10^{-16}
	10^{2}	10^{2}	10^{2}	$-0.7422665165\times10^{-3}$	0.2×10^{-16}
	10^{1}	10^{2}	10^{3}	$-0.1514006209\times10^{-3}$	-0.8×10^{-16}
	10^{3}	10^{3}	10^{3}	$0.5202463403\times10^{-4}$	-0.8×10^{-16}
	10^{5}	10^{4}	10^{3}	$-0.3663436948\times10^{-5}$	0.3×10^{-16}
3	10^{-5}	10^{-5}	10^{-5}	0.9078529274	-0.1×10^{-15}
	10^{-5}	10^{-4}	10^{-3}	1.361779390	-0.2×10^{-15}
	10^{-4}	10^{-4}	10^{-4}	1.361779261	0.2×10^{-15}
	10^{-3}	10^{-3}	10^{-3}	1.361766327	0.4×10^{-15}
	10^{-2}	10^{-2}	10^{-2}	1.360473397	0.4×10^{-15}
	10^{-1}	10^{-2}	10^{-3}	1.332741143	0
	10^{-1}	10^{-1}	10^{-1}	1.235652336	0.2×10^{-15}
	1	1	1	$-0.3190631567\times10^{-1}$	-0.2×10^{-15}
	10^{1}	10^{1}	10^{1}	$-0.1528018422\times10^{-1}$	0.5×10^{-16}
	10^{2}	10^{2}	10^{2}	$-0.1021957343\times10^{-2}$	0.6×10^{-16}
	10^{1}	10^{2}	10^{3}	$-0.1988284129\times10^{-3}$	-0.2×10^{-17}
	10^{3}	10^{3}	10^{3}	$0.1567941374\times10^{-3}$	-0.5×10^{-16}
	10^{5}	10^{4}	10^{3}	$-0.1442495824\times10^{-5}$	0.2×10^{-15}

where

$$P(v)=\begin{bmatrix}\lambda v_1^2 & v_1v_2 & v_1v_3\\ v_1v_2 & \lambda v_2^2 & v_2v_3\\ v_1v_3 & v_3v_2 & \lambda v_3^2\end{bmatrix}.$$

The matrix $P(v)$ can be written in the spherical coordinates as follows

$$P(r\cos(\varphi)\sin(\theta),r\sin(\varphi)\sin(\theta),r\cos(\theta))=r^2R(\varphi,\theta),$$

$$R(\varphi,\theta)=\begin{bmatrix}\lambda\cos^2(\varphi)\sin^2(\theta) & \cos(\varphi)\sin(\varphi)\sin^2(\theta) & \cos(\varphi)\sin(\theta)\cos(\theta)\\ \cos(\varphi)\sin(\varphi)\sin^2(\theta) & \lambda\sin^2(\varphi)\sin^2(\theta) & \sin(\varphi)\sin(\theta)\cos(\theta)\\ \cos(\varphi)\sin(\theta)\cos(\theta) & \sin(\varphi)\sin(\theta)\cos(\theta) & \lambda\cos^2(\theta)\end{bmatrix}.$$

The solution of (33) and (34) can be found in the form

$$\widetilde{\mathbf{u}}^m=Q\mathbf{v}^m, \tag{35}$$

where Q is a nonsingular matrix diagonalizing R, i.e. $Q^{-1}RQ=diag\,(k_1,k_2,k_3)$; $\mathbf{v}^m=(v_1^m,v_2^m,v_3^m)$ is a vector function, whose components are defined by

$$v_j^m=[Q^{-1}\mathbf{e}^m]_j\sin\left(rt\frac{\sqrt{k_j(c_{2323}+c_{1122})+c_{2323}}}{\sqrt{\rho}}\right)\times\frac{1}{r\sqrt{\rho(k_j(c_{2323}+c_{1122})+c_{2323})}},\quad j=1,2,3. \tag{36}$$

Using (35) and (36), we have computed the values of the components of $\widetilde{\mathbf{u}}^k$.

On the other hand, applying our method, we have computed the values of $\widetilde{G}_j^m$. Their comparison is presented in the Tables 2 and 3 for different values of θ and φ. The values of $\widetilde{u_3}^3$ and $\widetilde{G}_3^3$ computed by formula (35) and (36) and our method are almost the same (difference between values is less or equal to 10^{-16}).

4.2. Comparison of the values of the displacements

In this Section we describe the computational experiments, which confirm the correctness of our method. For the numerical computation of (24) and (25) in MATLAB we have replaced the $3D$ integration over the whole space R^3 by the integration over the bounded domain $(-A,A)\times(-A,A)\times(-A,A)$ and then approximated $3D$ integrals over this bounded domain by the triple sums with $A=40$ and $\Delta v=0.5$.

Example 1. In this example we consider an isotropic solid with wave speed quotient $C_L/C_T=2$, ($\mu=1$, $\lambda=2$ (10^{10} Pa), $\rho=0.75$ (10^3 kg/m^3)) similar to Wang and Achenbach (1994) and Payton (1983). Using formula (24) and our method, we have computed $\mathbf{u}^3(x,t)$ for

$$f(t)=\theta(t)t^2\exp(-3t^2). \tag{37}$$

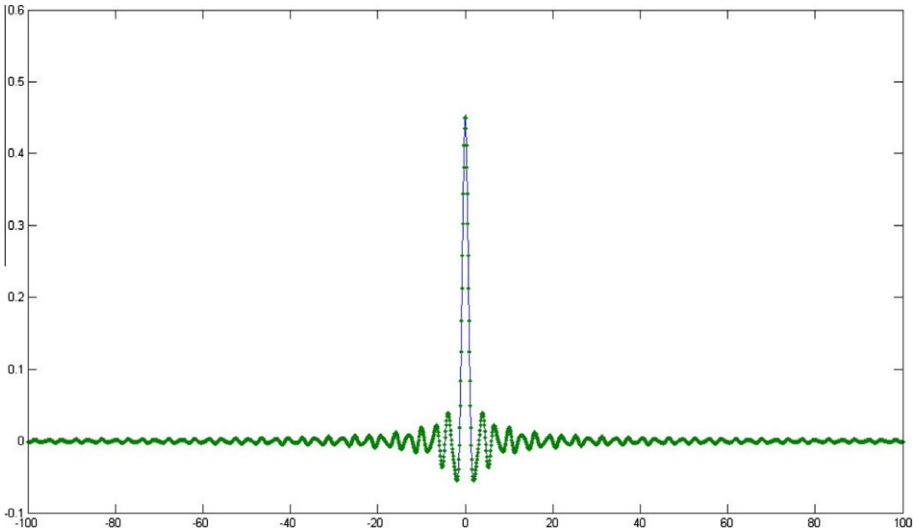

Fig. 1. Graphs of $\widetilde{G}_3^3(z,z,z,1)$ and $\widetilde{E}_3^3(z,z,z,1)$. The dotted line represents $\widetilde{E}_3^3(z,z,z,1)$ computed by (32) and continuous line represents $\widetilde{G}_3^3(z,z,z,1)$ computed by our method.

Table 2
The accuracy of computing $\widetilde{G}_3^3(r\cos\varphi\sin\theta, r\sin\varphi\sin\theta, \cos\theta, t)$ in Cubic material Gold. $\theta = \pi/4$, $\varphi = \pi/4$.

t	r	$\widetilde{G}_3^3(r\cos\varphi\sin\theta, r\sin\varphi\sin\theta, \cos\theta, t)$ (our method solution)	$\lvert\widetilde{G}_3^3 - \widetilde{u}_3^3\rvert$
1	10^{-5}	$0.5181347150 \times 10^{-1}$	0.7×10^{-17}
	10^{-3}	$0.5181346625 \times 10^{-1}$	0.7×10^{-17}
	10^{-2}	$0.5181294599 \times 10^{-1}$	0.7×10^{-17}
	10^{-1}	$0.5176094796 \times 10^{-1}$	0.7×10^{-17}
	1	$0.4683274640 \times 10^{-1}$	0.3×10^{-16}
	10^{1}	$-0.3776090096 \times 10^{-2}$	0.1×10^{-16}
	10^{2}	$0.1004035944 \times 10^{-2}$	0.9×10^{-18}
	10^{3}	$-0.4247308202 \times 10^{-5}$	0.6×10^{-17}
	10^{4}	$0.9005026217 \times 10^{-5}$	0.6×10^{-17}
	10^{5}	$0.2902583843 \times 10^{-6}$	0.4×10^{-19}
2	10^{-5}	0.1036269430	0.1×10^{-16}
	10^{-3}	0.1036269010	0.1×10^{-16}
	10^{-2}	0.1036227390	0.3×10^{-16}
	10^{-1}	0.1032074310	0.3×10^{-16}
	1	$0.6967412745 \times 10^{-1}$	0.3×10^{-16}
	10^{1}	$0.3717127055 \times 10^{-2}$	0.3×10^{-16}
	10^{2}	$-0.5759499033 \times 10^{-3}$	0.6×10^{-17}
	10^{3}	$0.4317120665 \times 10^{-4}$	0.2×10^{-16}
	10^{4}	$-0.5675042069 \times 10^{-5}$	0.2×10^{-17}
	10^{5}	$-0.8007901586 \times 10^{-6}$	0.6×10^{-17}
3	10^{-5}	0.1554404145	0.3×10^{-16}
	10^{-3}	0.1554402726	0.3×10^{-16}
	10^{-2}	0.1554262262	0.6×10^{-16}
	10^{-1}	0.1540283568	0
	1	$0.6726515489 \times 10^{-1}$	0.4×10^{-16}
	10^{1}	$-0.2466359996 \times 10^{-2}$	0.3×10^{-16}
	10^{2}	$-0.6480017032 \times 10^{-3}$	0.5×10^{-17}
	10^{3}	$0.6774514498 \times 10^{-4}$	0.2×10^{-16}
	10^{4}	$0.6053459816 \times 10^{-6}$	0.1×10^{-16}
	10^{5}	$0.9771328096 \times 10^{-6}$	0.1×10^{-16}

Table 3
The accuracy of computing $\widetilde{G}_3^3(r\cos\varphi\sin\theta, r\sin\varphi\sin\theta, \cos\theta, t)$ in Cubic material Gold. $\theta = \pi/3$, $\varphi = \pi/6$.

t	r	$\widetilde{G}_3^3(r\cos\varphi\sin\theta, r\sin\varphi\sin\theta, \cos\theta, t)$ (our method solution)	$\lvert\widetilde{G}_3^3 - \widetilde{u}_3^3\rvert$
1	10^{-5}	$0.5181347150 \times 10^{-1}$	0.7×10^{-17}
	10^{-3}	$0.5181346793 \times 10^{-1}$	0.7×10^{-17}
	10^{-2}	$0.5181311389 \times 10^{-1}$	0.7×10^{-17}
	10^{-1}	$0.5177772649 \times 10^{-1}$	0.7×10^{-17}
	1	$0.4839866039 \times 10^{-1}$	0
	10^{1}	$-0.5639674713 \times 10^{-2}$	0.2×10^{-17}
	10^{2}	$0.1078342276 \times 10^{-2}$	0.1×10^{-16}
	10^{3}	$-0.5230149370 \times 10^{-4}$	0.8×10^{-17}
	10^{4}	$0.7411610940 \times 10^{-5}$	0.5×10^{-17}
	10^{5}	$0.1062259319 \times 10^{-5}$	0.6×10^{-17}
2	10^{-5}	0.1036269430	0.1×10^{-16}
	10^{-3}	0.1036269144	0.3×10^{-16}
	10^{-2}	0.1036240821	0
	10^{-1}	0.1033413801	0
	1	$0.7978506975 \times 10^{-1}$	0
	10^{1}	$0.6951135990 \times 10^{-2}$	0.9×10^{-17}
	10^{2}	$-0.5732330819 \times 10^{-3}$	0.2×10^{-16}
	10^{3}	$-0.6228880994 \times 10^{-4}$	0.2×10^{-16}
	10^{4}	$-0.3912555058 \times 10^{-6}$	0.1×10^{-16}
	10^{5}	$0.8733233501 \times 10^{-6}$	0.3×10^{-16}
3	10^{-5}	0.1554404145	0
	10^{-3}	0.1554403180	0.3×10^{-16}
	10^{-2}	0.1554307593	0
	10^{-1}	0.1544788695	0
	1	$0.9068320067 \times 10^{-1}$	0.1×10^{-16}
	10^{1}	$-0.4472771962 \times 10^{-2}$	0.6×10^{-17}
	10^{2}	$-0.4509680105 \times 10^{-3}$	0.6×10^{-16}
	10^{3}	$0.2108162828 \times 10^{-4}$	0.2×10^{-16}
	10^{4}	$-0.2901061125 \times 10^{-5}$	0.3×10^{-16}
	10^{5}	$-0.3033165442 \times 10^{-6}$	0.5×10^{-16}

On the other hand there exists the explicit formulae for the components of the solution $\mathbf{u}^3(x,t)$ of (7) and (8) for the case of homogeneous isotropic solids (see Aki and Richards (1980)). From these formulae we have found for $u_3^3(0,0,z,t)$ and $u_3^3\left(\sqrt{6}z/4,\sqrt{6}z/4,z/2,t\right)$:

$$u_3^3(0,0,z,t)=\frac{1}{2\pi\rho|z|^3}\int_{|z|/C_L}^{|z|/C_T}\tau\theta(t-\tau)(t-\tau)^2\exp(-3(t-\tau)^2)d\tau+\frac{1}{4\pi\rho C_L^2|z|}\theta\left(t-\frac{|z|}{C_L}\right)\left(t-\frac{|z|}{C_L}\right)^2\times\exp\left(-3\left(t-\frac{|z|}{C_L}\right)^2\right),\tag{38}$$

$$u_3^3\left(\frac{\sqrt{6}}{4}z,\frac{\sqrt{6}}{4}z,\frac{z}{2},t\right)=-\frac{1}{16\pi\rho|z|^3}\int_{|z|/C_L}^{|z|/C_T}\tau\theta(t-\tau)(t-\tau)^2\times\exp(-3(t-\tau)^2)d\tau+\frac{1}{16\pi\rho C_L^2|z|}\theta\left(t-\frac{|z|}{C_L}\right)\left(t-\frac{|z|}{C_L}\right)^2\times\exp\left(-3\left(t-\frac{|z|}{C_L}\right)^2\right)+\frac{3}{16\pi\rho C_T^2|z|}\theta\left(t-\frac{|z|}{C_T}\right)\left(t-\frac{|z|}{C_T}\right)^2\times\exp\left(-3\left(t-\frac{|z|}{C_T}\right)^2\right).\tag{39}$$

The function $f(t)$ of the form (37) has been taken from the paper Wang and Achenbach (1994) to compare the results of our computation with the results presented in the paper Wang and Achenbach (1994). The graphs of functions $u_3^3(0,0,z,t)$ and $u_3^3\left(\sqrt{6}z/4,\sqrt{6}z/4,z/2,t\right)$ for $t=5\sqrt{\rho/\mu}$ obtained by our method and by explicit presentations (38) and (39) are presented in Figs. 2, 3 and have excellent agreement.

Example 2. In this example we consider the isotropic material silica (SiO_2) and in Eq. (7) we take $m=1$, $f(t)=\theta(t)$, where $\theta(t)$ is the Heaviside step function. Using our method, the values of matrices

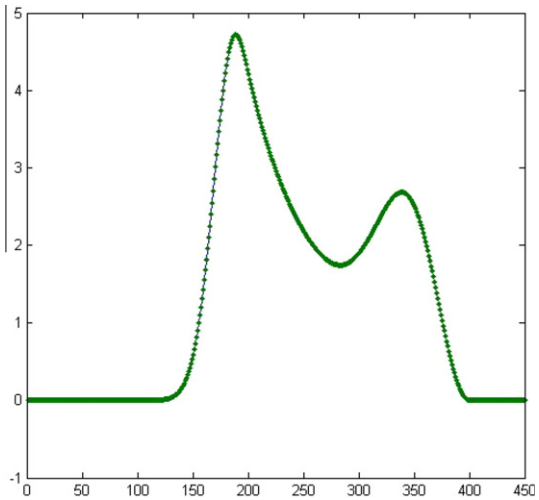

Fig. 2. Graphs of the third component $u_3^3(0,0,z,t)$ of solutions (7) and (8) for $f(t)=\theta(t)t^2\exp(-3t^2)$ at $t=5\sqrt{\frac{\rho}{\mu}}$ for an isotropic solid with wave speed quotient $C_L/C_T=2$. The dotted line represents analytical solution found by (38). The continuous line represents our method.

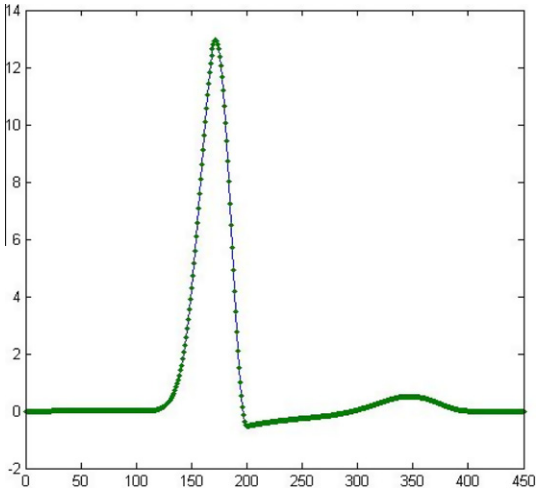

Fig. 3. Graphs of the third component $u_3^3\left(\sqrt{6}z/4,\sqrt{6}z/4,z/2,t\right)$ of solutions (7) and (8) for $f(t)=\theta(t)t^2\exp(-3t^2)$ at $t=5\sqrt{\frac{\rho}{\mu}}$ for an isotropic solid with wave speed quotient $C_L/C_T=2$. The dotted line represents analytical solution found by (39). The continuous line represents our method.

$\mathcal{T}(v)$, $\mathcal{T}^*(v)$, $D(v)$ have been found and then from the formula (24) $\mathbf{u}^1(x,t)$ has been computed. On the other hand we have used the explicit formulae for the components of the solution $\mathbf{u}^1(x,t)$ of (7) and (8) for the case of homogeneous isotropic solids (Aki and Richards, 1980). From these formulae we have found the following presentations for $u_1^1(z,z,z,t)$ and $u_2^1(z,z,z,t)$:

$$u_1^1(z,z,z,t)=\frac{1}{12\sqrt{3}\pi\rho|z|}\left[\frac{1}{C_L^2}\theta\left(t-\frac{\sqrt{3}|z|}{C_L}\right)+\frac{2}{C_T^2}\theta\left(t-\frac{\sqrt{3}|z|}{C_T}\right)\right],\tag{40}$$

$$u_2^1(z,z,z,t)=\frac{1}{24\sqrt{3}\pi\rho|z|}\left(\frac{1}{C_T^2}-\frac{1}{C_L^2}\right)\quad\text{for}\quad t>\frac{\sqrt{3}|z|}{C_T};\tag{41}$$

$$u_2^1(z,z,z,t)=\frac{1}{24\sqrt{3}\pi\rho}\left(\frac{t^2}{|z|^3}-\frac{1}{|z|C_L^2}\right)\quad\text{for}\quad\frac{\sqrt{3}|z|}{C_L}<t<\frac{\sqrt{3}|z|}{C_T};\tag{42}$$

and $u_2^1(z,z,z,t)=0$ for $t<\frac{\sqrt{3}|z|}{C_L}$.

The graphs of the functions $u_1^1(z,z,z,t)$ and $u_2^1(z,z,z,t)$ for $t=1$ obtained by our method and by explicit formulae (40)–(42) are presented in Figs. 4, 5 and have excellent agreement.

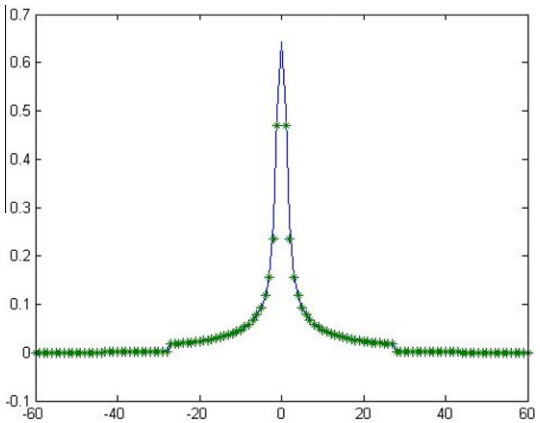

Fig. 4. Graphs of the first component $u_1^1(z,z,z,t)$ of solutions (7) and (8) for $f(t)=\theta(t)$ at $t=1$ for the isotropic solid silica (SiO_2). The line denoted by *** represents analytical solution found by formula (40). The line denoted by —— represents our method.

Example 3. In this example we consider the isotropic material silica (SiO_2). We take $m = 1$ and $f(t) = \delta(t)$ in Eq. (7), where $\delta(t)$ is the Dirac delta function. Using formula (25) and our method, $\mathbf{G}^1(x,t)$, i.e. the first column of the fundamental solution has been found. On the other hand we have used the explicit formulae (26)–(28). For drawing the graphs of the components of $\mathbf{G}^1(x,t)$ the singular terms $\delta(t-|x|/C_T)$ and $\delta(t-|x|/C_L)$ were replaced by $\frac{1}{2\sqrt{\pi\varepsilon}}\exp\left[-(t-|x|/C_T)^2/(4\varepsilon)\right]$ and $\frac{1}{2\sqrt{\pi\varepsilon}}\exp\left[-(t-|x|/C_L)^2/(4\varepsilon)\right]$ with $\varepsilon = 0.0001$, respectively.

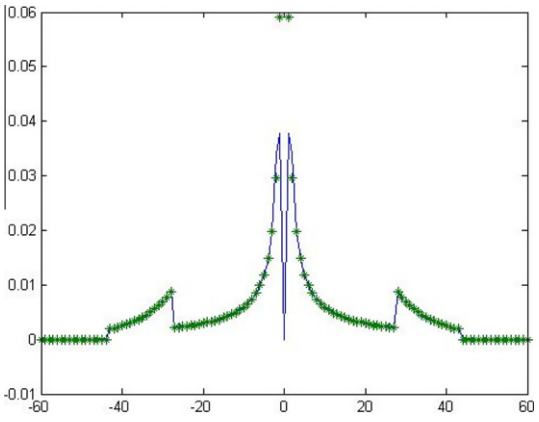

Fig. 5. Graphs of the second component $u_2^1(z,z,z,t)$ of solutions (7) and (8) for $f(t) = \theta(t)$ at $t = 1$ for the isotropic solid silica (SiO_2). The line denoted by $***$ represents analytical solution found by formulae (41) and (42). The line denoted by —— represents our method.

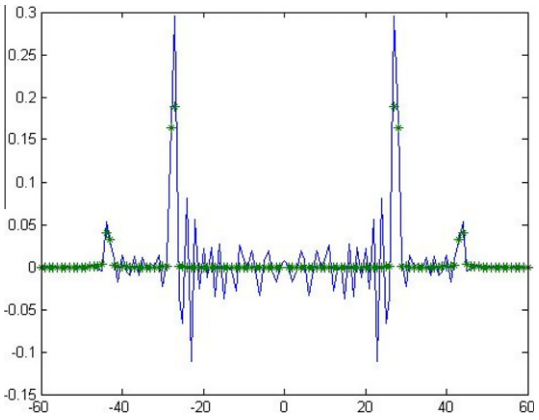

Fig. 6. Graphs of the first component $G_1^1(z,z,z,t)$ of solutions (7) and (8) for $f(t) = \delta(t)$ at $t = 1$ for the isotropic solid Silica (SiO_2). The line denoted by $***$ represents analytical solution found by formula (26), where $\delta(t)$ is approximated by $\exp[-t^2/(4\varepsilon)]/(2\sqrt{\pi\varepsilon}), \varepsilon = 0.0001$. The line denoted by —— represents our method.

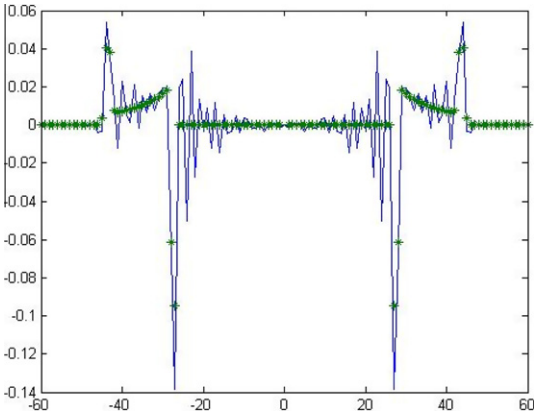

Fig. 7. Graphs of the second component $G_2^1(z,z,z,t)$ of solutions (7) and (8) for $f(t) = \delta(t)$ at $t = 1$ for the isotropic solid silica (SiO_2). The line denoted by $***$ represents analytical solution found by formula (27), where $\delta(t)$ is approximated by $\exp\left[-t^2/(4\varepsilon)\right]/(2\sqrt{\pi\varepsilon}), \varepsilon = 0.0001$. The line denoted by —— represents our method.

The graphs of functions $G_1^1(z,z,z,t)$ and $G_2^1(z,z,z,t)$ for $t = 1$ obtained by our method and by formulae (26)–(28) are presented in Figs. 6, 7. The curves of graphs $G_1^1(z,z,z,1)$ and $G_2^1(z,z,z,1)$, obtained by our method, fluctuate around curves of graphs of the functions $G_1^1(z,z,z,1)$ and $G_2^1(z,z,z,1)$, obtained by formulae (26)–(28). We can see in Figs. 6 and 7 that all peaks of graphs have the same positions and similar magnitudes.

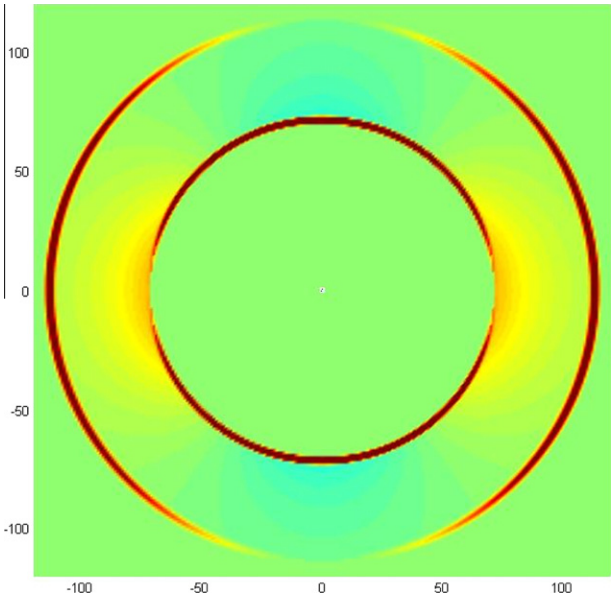

Fig. 8. The map surface plot of 3D surface $z = G_1^1(x_1,0,x_3,1.5)$, where $G_1^1(x_1,x_2,x_3,t)$ is computed by formula (26) for the isotropic elastic solid Silica (SiO_2); the Dirac delta function $\delta(t)$ is approximated in (26) by $\exp\left[-t^2/(4\varepsilon)\right]/(2\sqrt{\pi\varepsilon}), \varepsilon = 0.0001$.

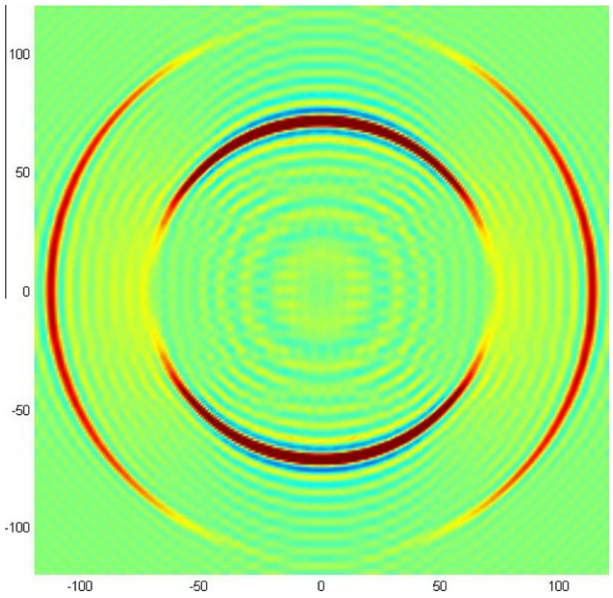

Fig. 9. The map surface plot of 3D surface $z = G_1^1(x_1,0,x_3,1.5)$, where $G_1^1(x_1,x_2,x_3,t)$ is computed for the isotropic elastic solid Silica (SiO_2).

Taking into account that $\mathbf{G}^m(x,t)$ is the elastic field arising from the pulse source $\mathbf{e}^m\delta(x)\delta(t)$ we can compute and visualize behavior of the elastic field at fixed time on a fixed plane, for example, on the plane $x_2 = 0$ at $t = 1.5$. The graphs of $G_1^1(x_1,0,x_3,1.5)$, obtained by formula (26) and by our method, are presented in Figs. 8 and 9, respectively. In these Figures the horizontal axis is x_1 and vertical axis is x_2. The graphs of these Figures mean the view from the top of the magnitude axis of G_1^1 and different colors correspond to different magnitudes. In these Figures we see clearly two fronts related to longitudinal and transverse waves, that propagate perpendicular to each other.

4.3. The images of wave propagation in general anisotropic materials

In this section two homogeneous elastic solids with general structure of anisotropy are considered.

4.3.1. The solid of monoclinic structure: sodium thiosulfate ($Na_2S_2O_3$)

The density $\rho = 1.7499$ kg/cm^3 and elastic constants are defined (see, for example, Hearmon, 1956) by

$$
\begin{aligned}
&c_{1111} = 0.3323, \quad c_{1122} = c_{2211} = 0.1814,\\
&c_{1133} = c_{3311} = 0.1875,\\
&c_{1113} = c_{1311} = 0.0225,\\
&c_{2222} = 0.2953, \quad c_{2233} = c_{3322} = 0.1713,\\
&c_{2213} = c_{1322} = 0.0983, \quad c_{3333} = 0.459,\\
&c_{3313} = c_{1333} = -0.0678, \quad c_{2323} = 0.0569,\\
&c_{2312} = c_{1223} = -0.0268, \quad c_{1313} = 0.107,\\
&c_{1212} = 0.0598 \text{ (GPa)}.
\end{aligned}
$$

Other elastic constants are equal to zero.

4.3.2. The solid of triclinic structure: Copper Sulphate Pentahydrate

The density $\rho = 2.649$ kg/cm^3 and elastic moduli are defined (see, for example, Brown et al., 2006) by

$$
\begin{aligned}
&c_{1111} = 5.65, \quad c_{1122} = c_{2211} = 2.65,\\
&c_{1133} = c_{3311} = 3.21, \quad c_{1123} = c_{2311} = -0.33,\\
&c_{1113} = c_{1311} = -0.08, \quad c_{1112} = c_{1211} = -0.39,\\
&c_{2222} = 4.33, \quad c_{2233} = c_{3322} = 3.47,\\
&c_{2223} = c_{2322} = -0.07, \quad c_{2213} = c_{1322} = -0.21,\\
&c_{2212} = c_{1222} = 0.02, \quad c_{3333} = 5.69,\\
&c_{3323} = c_{2333} = -0.44, \quad c_{3313} = c_{1333} = -0.21,\\
&c_{3312} = c_{1233} = -0.16, \quad c_{2323} = 1.73,\\
&c_{2313} = c_{1323} = 0.09, \quad c_{2312} = c_{1223} = 0.03,\\
&c_{1313} = 1.22, \quad c_{1312} = c_{1213} = -0.26,\\
&c_{1212} = 1 \text{ (GPa)}.
\end{aligned}
$$

For the computational experiments we have taken Eq. (7) with $f(t) = \delta(t)$. The goal of this experiment is to derive the fundamental solution of elastodynamics and to obtain the graphic presentations of its elements, using formula (25), our method and MATLAB tools. The physical meaning of mth column of the fundamental solution is the vector of displacement depending on the position (i.e. space variables x_1, x_2, x_3) and the time variable t, arising from the pulse point force of the form $\mathbf{e}^m\delta(x)\delta(t)$ in the considered elastic anisotropic solid. The graphic presentation of the components of this displacement in points of the space gives a possibility to observe the wave propagation phenomenon, in particular, wave fronts arising from pulse point sources at different times in general anisotropic solids.

Using our method we have computed numerically the components of $\mathbf{G}^m(x,t)$.

Fig. 10 presents the first component of the displacement $\mathbf{G}^1(x_1,0,x_3,t)$ at $t = 4$. Here the horizontal and vertical axes are x_1 and x_3, respectively. Fig. 10 presents a view from the top of the magnitude axis G_1^1 (i.e. the view of the surface $z = G_1^1(x_1,0,x_3,4)$ from the top of z axis).

Similar, Fig. 11 presents the second component of the displacement $\mathbf{G}^1(x_1,x_2,0,t)$ at $t = 5$. Here the horizontal and vertical axes are x_1 and x_2, respectively. Fig. 12 presents the third component of the displacement $\mathbf{G}^1(x_1,0,x_3,t)$ at the time $t = 4$. Here the horizontal and vertical axes are x_1 and x_3, respectively.

In Figs. 10–12 one can see the behavior of the components of the elastic field in the monoclinic solid Sodium Thiosulfate, arising

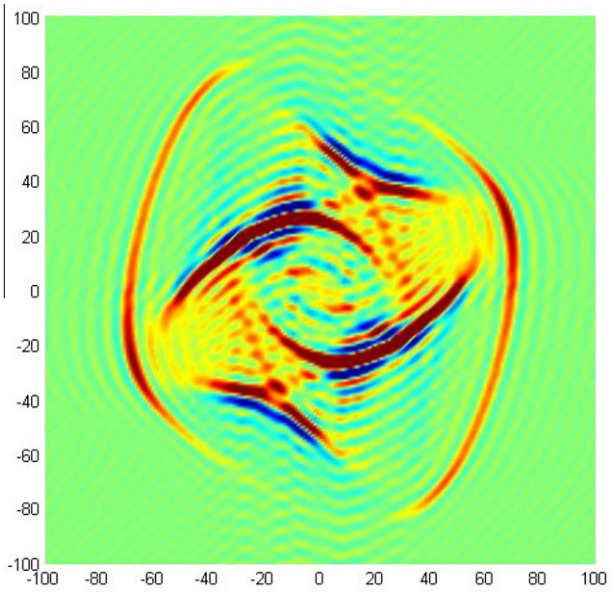

Fig. 10. The map surface plot of 3D surface $z = G_1^1(x_1,0,x_3,4)$, where $G_1^1(x_1,x_2,x_3,t)$ is computed for Sodium Thiosulfate (monoclinic structure of anisotropy).

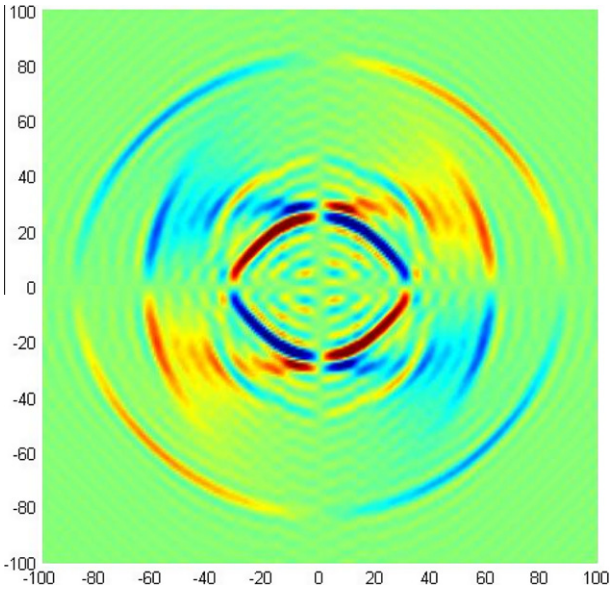

Fig. 11. The map surface plot of 3D surface $z = G_2^1(x_1,x_2,0,5)$, where $G_2^1(x_1,x_2,x_3,t)$ is computed for Sodium Thiosulfate (monoclinic structure of anisotropy).

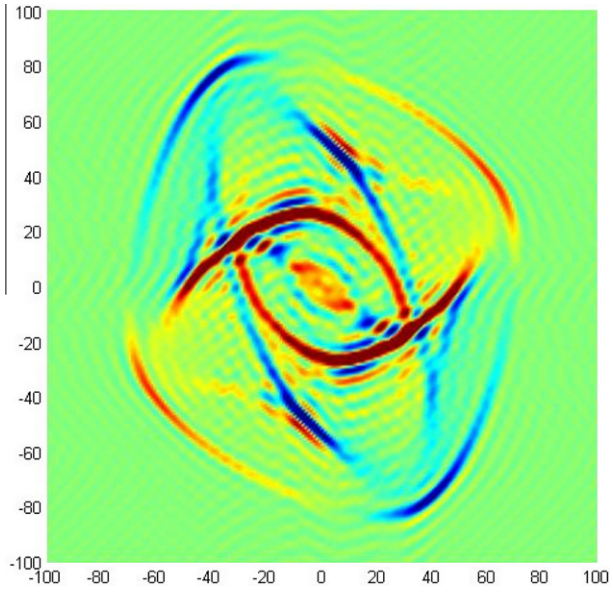

Fig. 12. The map surface plot of 3D surface $z = G_3^1(x_1, 0, x_3, 4)$, where $G_3^1(x_1, x_2, x_3, t)$ is computed for Sodium Thiosulfate (monoclinic structure of anisotropy).

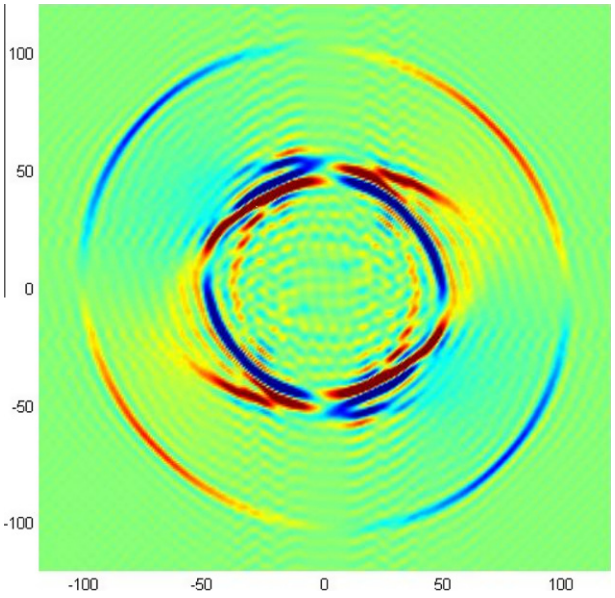

Fig. 13. The map surface plot of 3D surface $z = G_1^3(x_1, 0, x_3, 1.75)$, where $G_1^3(x_1, x_2, x_3, t)$ is computed for Copper Sulphate Pentahydrate (triclinic structure of anisotropy).

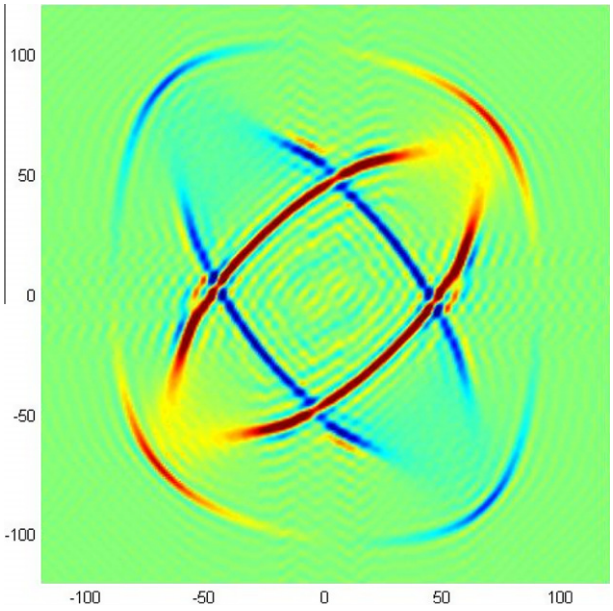

Fig. 14. The map surface plot of 3D surface $z = G_2^3(x_1, 0, x_3, 1.75)$, where $G_2^3(x_1, x_2, x_3, t)$ is computed for Copper Sulphate Pentahydrate (triclinic structure of anisotropy).

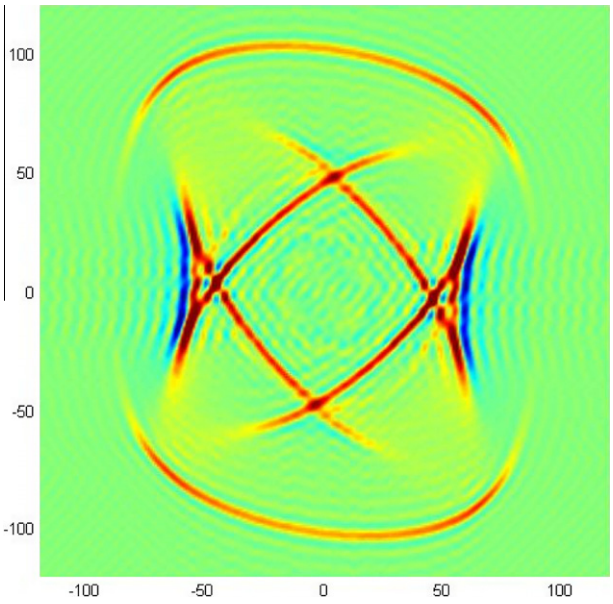

Fig. 15. The map surface plot of 3D surface $z = G_3^3(x_1, 0, x_3, 1.75)$, where $G_3^3(x_1, x_2, x_3, t)$ is computed for Copper Sulphate Pentahydrate (triclinic structure of anisotropy).

from the pulse point force $\mathbf{e}^1\delta(x)\delta(t)$. One can see the peculiar forms of the traces of wave fronts on the planes $x_2 = 0$, $x_3 = 0$.

Fig. 13 presents the first component of the displacement $\mathbf{G}^3(x_1,0,x_3,t)$ at $t = 1.75$. Fig. 14 presents the second component of the displacement $\mathbf{G}^3(0,x_2,x_3,t)$ at $t = 1.75$. Fig. 15 presents the third component of the displacement $\mathbf{G}^3(0,x_2,x_3,t)$ at the time $t = 1.75$. Figs. 13–15 are the screen shots of $2-D$ level plots of the surfaces $G_1^3(x_1, 0, x_3, 1.75)$, $G_2^3(0, x_2, x_3, 1.75)$, $G_3^3(0, x_2, x_3, 1.75)$, respectively. This is a view from the top of z-axis (the plan). In Figs. 13–15 one can see the behavior of components of the elastic field in the triclinic solid Copper Sulphate Pentahydrate, arising from the pulse point force $\mathbf{e}^3\delta(x)\delta(t)$ with the peculiar forms of the traces of wave fronts which we observe on the planes $x_1 = 0$, $x_2 = 0$.

5. Conclusion

In the paper the new method of the approximate calculation of the displacement, arising from the directional point force is general anisotropic materials, is suggested. This method consists in the following: the second order equations of elastodynamics have been written in terms of the Fourier transform with respect to the space variables as a system of the ordinary differential equations of the second order with coefficients depending on the Fourier parameters.

The solution of the obtained system has been derived by the matrix transformations and technique of the ordinary differential

equations. After that, the inverse Fourier transformation has been applied numerically to this solution.

Several types of computational experiments have been done for validation of the method. The results of the calculation of the Fourier transform of the fundamental solution have been compared with the values, obtained from the explicit formulae for the isotropic material and anisotropic material of the cubic structure. The comparison has demonstrated the high level of coincidence.

The calculated values of the displacement vector have been compared with values obtained by the method of Wang and Achenbach (1994), Payton (1983), and with the values, derived from explicit formula for the isotropic solid Silica, derived by Aki and Richards (1980). The comparison demonstrates the high level of co-ordination of values.

The computational examples have confirmed the robustness of the suggested method, which can be used for drawing images of the elastic wave propagations in materials with general anisotropic structures.

References

Aki, K., Richards, P.G., 1980. Quantitative Seismology. Theory and Methods. Freeman and company, San Francisco.

Barton, G., 1991. Elements of Green's Functions and Propagation. Oxford University Press, New York.

Berger, J.R., Tewary, V.K., 1996. Green's Functions and Boundary Element Analysis for Modelling of Mechanical Behavior of Advanced Materials. National Institute of Standarts and Technology, Special Publication 910, Boulder, Colorado.

Brown, J.M., Abramson, E.H., Angel, R.J., 2006. Triclinic elastic constants for low albite. Phys. Chem. Minerals 33, 256–265.

Burridge, R., Chadwick, P., Norris, A.N., 1993. Fundamental elastodynamic solutions for anisotropic media with ellipsoidal slowness surfaces. Proc. Roy. Soc. London Ser. A 440 (1910), 655–668.

Carcione, J.M., 2001. Wave Fields in Real media: Wave Propagation in Anisotropic. Anelastic and Porous media. Pergamon, Amsterdam.

Carrer, J.A.M., Mansur, W.J., 1999. Stress and velocity in 2D transient elastodynamic analysis by the boundary element method. Eng. Anal. Boundary Elem. 23, 233–245.

Chang, J.H., Wu, D.J., 2003. Finite element calculation of elastodynamic stress field around a notch tip via contour integrals. Int. J. Solids Struct. 40, 1189–1202.

Dauksher, W., Emery, A.F., 2000. The solution of elastostatic and elastodynamic problems with Chebyshev spectral finite elements. Comput. Methods Appl. Mech. Eng. 88, 217–233.

Dieulesaint, E., Royer, D., 1980. Elastic Waves in Solids. Applications to Signal Processing. John Wiley and Sons, Chichester.

Dieulesaint, E., Royer, D., 2000. Elastic Waves in Solids I. Free and Guided Propagation. Springer-Verlag, Berlin, Heidelberg.

Ehrenpreis, L., 1960. Solution of some problems of division. IV. Invertible and elliptic operators. Amer. J. Math. 82, 522–588.

Fedorov, F.I., 1968. Theory of Elastic Waves in Crystals. Plenum Press, New York.

Freund, L.B., 1998. Dynamic Fracture Mechanics. Cambridge University Press.

Garg, N.R., Goel, A., Miglani, A., Kumar, R., 2004. Elastodynamic response of an anisotropic medium due to a line-load. Earth Planets Space 56, 407–417.

Hachemi, M.E., Callé, S., Remenieras, J.P., 2008. Transient displacement induced in shear wave elastography: comparison between analytical results and ultrasound measurements. Ultrasonics 44, e221–e225.

Harada, K., Sasahara, H., 2009. Effect of dynamic response and displacement/stress amplitude on ultrasonic vibration cutting. J. Mater. Process. Technol. 209, 4490–4495.

Hearmon, R.F.S., 1956. Adv. Phys. 5, 323–382.

Hormander, L., 1963. Linear Partial Differential Operators. Springer, Berlin.

Khojasteh, A., Rahimian, M., Pak, R.Y.S., 2008. Three-dimensional dynamic Greens functions in transversely isotropic bi-materials. Int. J. Solids Struct. 45, 4952–4972.

Kocak, H., Yildirim, A., 2009. Numerical solution of 3D Green's function for the dynamic system of anisotropic elasticity. Phys. Lett. A 373, 3145–3150.

Malgrange, B., 1955–1956. Existence et approximation des solutions des équations aux dérivées partielles et des équations de convolution. (French) Ann. Inst. Fourier, Grenoble 6, 271–355.

Mansur, W.J., Loureiro, F.S., 2009. An efficient hybrid time-Laplace domain method for elastodynamic analysis based on the explicit Greens approach. Int. J. Solids Struct. 46, 3093–3102.

Mansur, W.J., Loureiro, F.S., Soares Jr., D., Dors, C., 2007. Explicit time-domain approach based on numerical Green's functions computed by finite differences-the ExGA family. J. Comput. Phys. 227, 851–870.

Moosavi, M.R., Khelil, A., 2009. Finite volume meshless local Petrov–Galerkin method in elastodynamic problems. Eng. Anal. Boundary Elem. 33, 1016–1021.

Payton, R.G., 1983. Elastic Wave Propagation in Transversely Isotropic Media. Martinus Nijhoff Publishers, The Hague.

Poruchikov, V.B., 1993. Methods of the Classical Theory of Elastodynamics. Springer, Berlin.

Rangelov, T.V., 2003. Scattering from cracks in an elasto-anisotropic plane. J. Theoret. Appl. Mech. 33, 55–72.

Rangelov, T.V., Manolis, G.D., Dineva, P.S., 2005. Elastodynamic fundamental solutions for certain families of 2d inhomogeneous anisotropic domains: basic derivations. Eur. J. Mech. A/Solids 24, 820–836.

Reed, M., Simon, B., 1975. Methods of Modern Mathematical Physics. II. Fourier Analysis, Self-Adjointness. Academic Press, New York.

Sladek, J., Sladek, V., Zhang, C., 2005. An advanced numerical method for computing elastodynamic fracture parameters in functionally graded materials. Comput. Mater. Sci. 32, 532–543.

Soares Jr., D., Mansur, W.J., 2005. A time domain FEM approach based on implicit Green's functions for nonlinear dynamic analysis. Int. J. Numer. Methods Eng. 62, 664–681.

Tewary, V.K., 1995. A computationally efficient representation for elastostatic and elastodynamic Green's functions for anisotropic solids. Phys. Rev. B 51, 15695–15702.

Ting, T.C.T., 1996. Anisotropic Elasticity: Theory and Applications. Oxford University Press, Oxford.

Ting, T.C.T., Barnett, D.M., Wu, J.J., 1990. Modern Theory of Anisotropic Elasticity and Applications. SIAM, Philadelphia.

Vavrycuk, V., 2001. Exact elastodynamic Green functions for simple types of anisotropy derived from higher-order ray theory. Stud. Geophys. Geod. 45, 67–84.

Vavrycuk, V., 2002. Asymptotic elastodynamic Green function in the kiss singularity in homogeneous anisotropic solids. Stud. Geophys. Geod. 46, 249–266.

Vera-Tudela, C.A.R., Telles, J.C.F., 2005. A numerical Greens function and dual reciprocity BEM method to solve elastodynamic crack problems. Eng. Anal. Boundary Elem. 29, 204–209.

Vladimirov, J.V.S., 1971. Equations of Mathematical Physics. Marcel Dekker, New York.

Vladimirov, V.S., 1979. Generalized Functions in Mathematical Physics. Mir Publishers, Moscow.

Wang, V.Y., Achenbach, J.D., 1994. Elastodynamic fundamental solutions for anisotropic solids. Geophys. J. Int. 118, 384–392.

Wang, V.Y., Achenbach, J.D., 1995. Three-dimensional time-harmonic elastodynamic Green's functions for anisotropic solids. Proc. R. Soc. London A449, 441–458.

Wang, X., Pan, E., Feng, W.J., 2007. Time-dependent Green's functions for an anisotropic bimaterial with viscous interface. Eur. J. Mech. A/Solids 26, 901–908.

Yakhno, V., Cerdik Yaslan, H., 2011. Computation of the time-dependent fundamental solution for equations of elastodynamics in general anisotropic media. Comput. Struct. 89, 646–655.

Yang, B., Pan, E., Tewary, V.K., 2004. Three-dimensional Greens functions of steady-state motion in anisotropic half-spaces and bimaterial. Eng. Anal. Boundary Elem. 28, 1069–1082.